DOI: 10.61782/fa.2023.0750

forum acusticum 2023

NUMERICAL AND EXPERIMENTAL INVESTIGATION OF A PHASE GRADIENT METASURFACE LINING

Giorgio Palma[1*] **Lara Flanagan**[2] **Lorenzo Burghignoli**[1] **John Kennedy**[3]

[1] Department of Civil, Computer Science and Aeronautical Technologies Engineering, University of Roma Tre, Italy

[2] Laboratoire d'Acoustique de l'Université du Maine, UMR CNRS 6613, Avenue Olivier Messiaen, 72085 Le Mans, France

[3] Department of Mechanical, Manufacturing and Biomedical Engineering, Trinity College Dublin, Ireland

ABSTRACT

This work presents an experimental and numerical study of a non-homogeneous acoustic treatment based on space-coiling unit cells. A modular phase gradient metasurface is used in the experimental analysis as a wall lining in a Grazing Impedance Tube. A metacontinuum reduced order model of the cells is used in FEM simulations to predict the experimental results. The experiments and the numerical analysis show a good agreement in terms of the predicted transmission coefficient spectrum for the selected benchmark problem. Although not optimized, the non-homogeneous acoustic treatment showed remarkable transmission loss in a wide range of frequencies, which can be explained by a subwavelength distribution of acoustic resonators with different resonance frequencies.

Keywords: *metamaterials, metasurfaces, acoustics*

1. INTRODUCTION

Metamaterials represent one of the most active research fields in classic mechanics, experiencing great interest from the scientific community in the last fifteen years. The term metamaterial is related to the possibility of engineered structures to produce responses, metabehaviours, hardly or not available in nature by conventional materials, due to their geometric features rather than their chemical compositions [1,2]. Acoustics is one of the fields that achieved the most proficuous applications of metamaterial concepts. Exotic effects such as negative dynamic mass and/or bulk modulus [3, 4], negative refractive index [5, 6], sound focusing [7, 8], and acoustic invisibility [9–16] are the most famous results so far obtained carefully designing the microstructures of the involved devices. The metabehaviours are achieved by the majority of acoustic metamaterials introducing local resonances at the working frequencies of the devices [17]. A particular class of metamaterials called Phase-Gradient Metasurfaces (PGMS) exploits acoustic phase delay distributions to induce anomalous reflection and refraction from boundaries [18,19]. The structures used to manipulate the wavefronts are of several shapes, and their thickness is typically sought to be subwavelength. A simple description of their functioning, regardless of the actual design, may associate the cells to off-resonance resonators in order to introduce a tailored delay in the reflected field in the complete range $0-2\pi$ (when the working frequency matches the resonant one, the delay introduced is $\pi/2$).

In this article, we studied the application of a metasurface as a wall treatment in a duct. The metasurface is composed of eight different cells whose phase delays sequentially differ by $\pi/4$. Experiments are conducted in a Grazing Impedance Tube to investigate the transmission coefficient spectrum of the metasurface sample manufactured with 3D fast prototyping technique. The experimental analysis is supported by analytic and numerical mod-

**Corresponding author*: *giorgio.palma@uniroma3.it.*

elling of the acoustic behaviour of the metasurface. A metafluid model for the unit cells is used and implemented in a finite element analysis of the lined duct. The results from the two approaches are compared and discussed.

2. METHODS

A space-coiling cell [19] is parametrised and used as a unit cell for building a PGMS metasurface. Figure 1 show a sketch of the geometry and its parametrization. Each cell is fully determined by the geometrical variables vector $\boldsymbol{\chi}_\mathrm{A} = [n_w \; w \; d \; l, \; a_x]$ where n_w identifies the number of bends of the channel in the cell, w is the thickness of the internal septa, all with the same length l, creating the folds, d is the width of the channel opening and height of each segment of the channel, which length is $l + d$, and a_y is the overall width of the cell. Sizes are completed with the definition of the overall height of the cell $a_y = n_w \; (d + w)$ and the thickness of the side walls $t = 0.5 \; (a_y - (d + l))$. Eight cells compose the metasurface that has been studied in the present article. Their design parameters are reported in Tab.1.

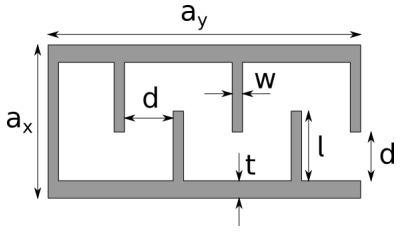

Figure 1. Geometry of the reference unit cell.

	#1	#2	#3	#4	#5	#6	7	#8
n_w	6	5	4	3	2	2	2	2
w (mm)	2	2	2	2	2	2	2	2
d (mm)	3	7	10	12	18	16	11	12
l (mm)	14	8	7	3	3	4	9	3
a_x (mm)	25	25	25	25	25	25	25	25

Table 1. Design variables of each cell, cfr. Fig. 1.

2.1 Manufacturing

The metasurface under study is built placing one element of each of the cells in Table 1 side by side from #1 to #8. The metasurface is manufactured by fused filament fabrication, which is a 3D printing process that uses a continuous filament of a thermoplastic material using a Creality Ender 3 printer. The accuracy of FDM-based printers is linked to the nozzle size; features less than this size cannot accurately be produced. In general, the layer line width and nozzle speed will also affect the accuracy of larger-scale geometric features, and the deviation from the specified dimensions can be of the order of two nozzle widths. In this case, the nozzle size was 0.4 mm. The 3D FDM additive manufacturing, hence, introduces uncertainties in the sizes of the manufactured metasurfaces, which should be accounted for when trying to match with the numerical results.

2.2 Metafluid model

The channels of the space-coiling structure have subwavelength width, being waveguides for the 0^{th} order acoustic mode. There always exists for a coiled cell an equivalent straight channel length, $l_{eq} = g(l)$, which is a function of the unfolded channel extension but generally differs from the purely geometric length. The equivalent length is the fundamental parameter of such cells, directly defining the expected phase delay introduced in the reflected field compared to a flat boundary $\Delta\Phi = \frac{4\pi l_{eq}}{\lambda_0}$ or, equivalently, the effective relative refractive index $n_{\mathrm{eff}} = l_{eq}/t$. The acoustic modelling of the cells is obtained in this work by means of an equivalent metafluid model [20–22]. An acoustic metafluid is a particular case of metacontinuum that behaves acoustically as a fluid due to the null shear modulus exhibited by its structure (or near-zero in practical realizations [23]), potentially including anisotropy in its response. Acoustic perturbations propagate in the most general metafluid following [16, 24]

$$-\frac{\partial^2 p}{\partial t^2} + c_{\mathrm{ref}}^2 \, \hat{\mathcal{K}} \, \nabla \cdot \left(\mathbf{Q} \, \hat{\boldsymbol{\varrho}}^{-1} \, \mathbf{Q} \, \nabla p \right) = 0 \qquad (1)$$

where $\boldsymbol{\varrho} = \hat{\boldsymbol{\varrho}} \varrho_{\mathrm{ref}}$ represents the anisotropic inertia of the material, $\mathcal{K} = \hat{\mathcal{K}} \mathcal{K}_{\mathrm{ref}}$, $\mathbf{Q}$ can be any symmetric tensor such that $\nabla \cdot \mathbf{Q} = 0$ and the Cauchy stress tensor for such a material is given by $\boldsymbol{\sigma} = -p \, \mathbf{Q}$; ϱ_{ref}, $\mathcal{K}_{\mathrm{ref}}$, and $c_{\mathrm{ref}} = \sqrt{\mathcal{K}_{\mathrm{ref}}/\varrho_{\mathrm{ref}}}$ are the reference density, bulk modulus, and speed of sound, respectively, which may be taken arbitrarily equal to the values for the hosting fluid ρ_0, $\rho_0 c_0^2$ and c_0, respectively. The volume occupied by the metafluid representing a cell can be chosen arbitrarily. It is here taken defining a metafluid cell as thick as the original one, $l_{mf} = a_y$, and as wide as the channel of each cell

$d_{mf} = d$. Following the Transformation Acoustics procedure [24], a coordinate transformation is set between the original domain $\Omega(X, Y, Z)$ (the equivalent straight channel) and the metafluid $\omega(x, y, z)$, through an invertible mapping $\Omega \rightarrow \omega$ defined by $\boldsymbol{\xi} = \chi(\boldsymbol{\Xi})$. Mapping the equivalent length in the metafluid thickness, we obtain

$$\begin{aligned} x &= X \\ y - y_0 &= \frac{l_{mf}}{l_{eq}}(Y - Y_0), \qquad Y_0 < Y < l_{eq} \\ z &= Z \end{aligned} \tag{2}$$

The components of the transformation gradient $\mathbf{F}$ are described as $f_{ij} = \partial\xi_i/\partial\Xi_j$, $\boldsymbol{\xi} = (x, y, z)$ and $\boldsymbol{\Xi} = (X, Y, Z)$. In the following, the problem is addressed under the simplifying hypothesis of inertial metafluid, a special case of the more general class of metacontinua that implies $\mathbf{Q} = \mathbf{I}$. In this case, the metacontinuum parameters are related to $\mathbf{F}$ by

$$\hat{\mathcal{K}} = \det \mathbf{F}, \quad \hat{\boldsymbol{\varrho}} = \det(\mathbf{F})(\mathbf{V}\mathbf{V}^{\mathrm{T}})^{-1} \tag{3}$$

with $\mathbf{V}^2 = \mathbf{F}\mathbf{F}^T$ The corresponding deformation gradient $\mathbf{F}$ is

$$\begin{aligned} \mathbf{F} &= \begin{bmatrix} f_{11} & 0 & 0 \\ 0 & f_{22} & 0 \\ 0 & 0 & f_{33} \end{bmatrix}, \\ f_{11} = 1, \quad f_{22} &= \frac{l_{ms}}{l_{eq}}, \quad f_{33} = 1 \end{aligned} \tag{4}$$

hence the metafluid is characterized by

$$\hat{\mathcal{K}} = f_{22}, \quad \hat{\boldsymbol{\varrho}} = f_{22} \begin{bmatrix} 1 & 0 & 0 \\ 0 & \frac{1}{f_{22}^2} & 0 \\ 0 & 0 & 1 \end{bmatrix} \tag{5}$$

The cells' equivalent lengths l_{eq} are obtained by introducing semiempirical linear corrections depending on some cell design parameters over the geometric length calculation of the zig-zag path inside the cells with sizes expressed in meters.

$$\begin{aligned} l_{eq} &= \sqrt{(d + w)^2 + a_x^2} + c_1 d + c_2 a_x + c_3 w + c_4, \\ c_1 &= -0.75, c_2 = 0.0409, c_3 = 0.9, c_4 = -0.0003 \end{aligned} \tag{6}$$

In addition, thermoviscous losses are accounted for in the metafluid domain introducing a complex-valued expression for the speed of sound originally introduced by Pierce [25]. When the considered channel is large enough for the boundary layers to occupy a small fraction of its cross-section, the dispersion relation can be approximated by

$$\begin{aligned} \frac{\omega}{c_{\text{ref}}} &= \frac{\omega}{c_0} + (1 - i)a_{\text{walls}} \\ a_{\text{walls}} &= \frac{1}{c_0 d_{\text{eq}}} \sqrt{\frac{\omega\eta}{2\rho_0}} \left(1 + \frac{\gamma - 1}{\sqrt{Pr}}\right) \end{aligned} \tag{7}$$

with η, d_{eq}, γ, and Pr being the dynamic viscosity of the reference fluid, the equivalent channel diameter, the ratio of the specific heats, and the Prandtl number, respectively.

2.3 Experimental analysis

For the experimental validation of the FDM printed metasurface, tests were conducted in a grazing incidence impedance tube at the LAUM, a schematic which represents the rig is shown in Fig 2. The tube consists of a rectangular cross-section of 40 mm$\times$ 50 mm; more details on the capabilities of the test bench are given in [26]. Acoustic sources can either be mounted upstream or downstream of the test section. There are anechoic terminations on either sides to limit reflections that can affect measurements. Three flush-mounted microphones are used to record the sound pressure in the duct located upstream u_i and downstream d_i of the metasurface sample. The distance from the first upstream and downstream microphones u_1 and d_1 to the metasurface sample is 118 mm. The position of the upstream and downstream microphones are as follows $x_{u_1} - x_{u_2} = x_{d_1} - x_{d_2} = 30$ mm and $x_{u_1} - x_{u_3} = x_{d_1} - x_{d_3} = 175$ mm. Measurements with acoustic sources were performed upstream and downstream of the sample through a sine sweep excitation ranging from 100 Hz to 4000 Hz with a 5 Hz step. At each frequency step, the acoustic pressure on each microphone is calculated by averaging the pressure value over 300 cycles. To assess the linear behaviour of the sample, incident sound pressure level of 100dB, 130dB and 140dB were chosen and maintained at these value as a function of frequency (error of $\pm$ 0.1 dB). Two different acoustic states are used to obtain the elements of the scattering matrix. In the first where there is an incident plane wave upstream of the sample to obtain $\tau^+$and r^+. In a second state with the incoming wave through an acoustic source located downstream of the sample to obtain $= \tau^-$and r^-.The use of three microphones upstream and downstream is an overdeterministic approach of the transmitted and reflected waves on either side of the lined section [27].

The measured transmission coefficient is used to compare the effectiveness of the model metasurface behaviour.

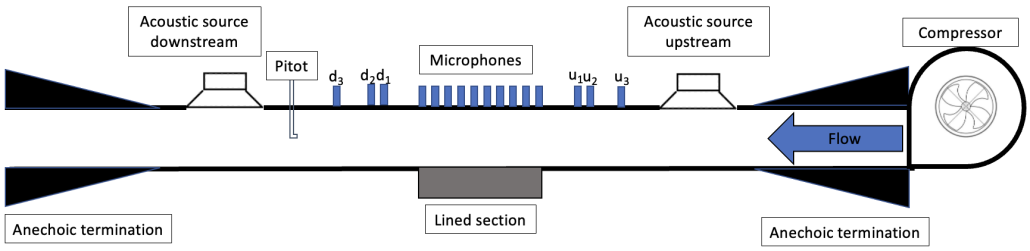

Figure 2. Schematic of the grazing incidence rig at LAUM

2.4 Numerical analysis

A schematic geometry representing the grazing impedance tube used in the experiments is used for numerical simulations. The numerical analysis is conducted in 2D, using the central section of the tube as a representative. The height of the numerical duct is the same as the real tube, and a convergence analysis has been performed on its length to avoid interference from the boundaries. The numerical analysis has been conducted assuming purely harmonic acoustic perturbations. The Fourier-transformed version of Eq. 1 is used in the cells' metafluid domains, along with the Helmholtz equation for the duct domain. A plane wave excitation is imposed at one end of the duct. The boundary conditions at the two ends are imposed for each simulation as needed for the evaluation of the transmission coefficient (as specified in Sec. 3), the other boundaries are imposed to be acoustically rigid. The complete geometry of the metasurface is also studied, using a narrow region acoustics model that implements Pierce's model for a complex speed of sound to account for viscous losses in small channels, and a classic linear lossless acoustic model solving for the Helmholtz equation in all the simulation domain, for comparison purposes. The respective weak formulations are implemented in a commercial FEM solver, and results are obtained for a frequency sweep from 100 Hz to 4000 Hz.

3. RESULTS

The experimental and numerical prediction comparison is presented in terms of the Transmission coefficient (τ) given by the metasurface in the duct. The numerical pro-

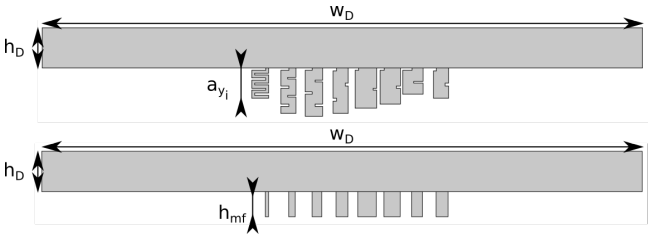

Figure 3. Schematic of the original geometry and with the metafluid used in the FEM simulations.

cedure to evaluate τ starts by calculating the four-pole parameters of the transfer matrix of the acoustic system, which links the average acoustic pressures and velocities on the inlet and outlet sections ($\bar{p}_1$,$\bar{p}_2$, and $\bar{u}_1$, $\bar{u}_2$, respectively, the bar meaning the average operation along the section)

$$\begin{bmatrix} \bar{p}_1 \\ \rho_0 c_0 \bar{u}_1 \end{bmatrix} = \begin{bmatrix} A\,B \\ C\,D \end{bmatrix} \begin{bmatrix} \bar{p}_2 \\ \rho_0 c_0 \bar{u}_2 \end{bmatrix} \tag{8}$$

The numerical evaluation of the four pole parameters can be done in two steps, using two different sets of boundary conditions at the inlet and outlet: A and C are obtained by imposing u_1=1 and u_2=0; inverting the assignment (u_1=0 and u_2=1) allows for the evaluation of B and D.

$$\begin{aligned} A &= \left.\frac{\bar{p}_1}{\bar{p}_2}\right|_{\substack{u_1=1\\u_2=0}}, \quad B = \left.\frac{\bar{p}_1 - A\bar{p}_2}{\rho_0 c_0}\right|_{\substack{u_1=0\\u_2=1}} \\ C &= \left.\frac{-\rho_0 c_0}{\bar{p}_2}\right|_{\substack{u_1=1\\u_2=0}}, \quad D = \left.\frac{-C\bar{p}_2}{\rho_0 c_0}\right|_{\substack{u_1=0\\u_2=1}} \end{aligned} \tag{9}$$

from which the transmission coefficient is evaluated

$$\tau = \frac{2}{|A + B + C + D|} \tag{10}$$

The same quantity is evaluated experimentally from the scattering matrix of the problem. The scattering matrix relates the scattered pressures p_3^+ and p_1^- to the incident pressures p_1^+ and p_3^- through the transmission and reflected coefficients in equation 11.

$$\begin{pmatrix} p_3^+ \\ p_1^- \end{pmatrix} = S \begin{pmatrix} p_1^+ \\ p_3^- \end{pmatrix} = \begin{bmatrix} \tau^+ & r^- \\ r^+ & \tau^- \end{bmatrix} \begin{pmatrix} p_1^+ \\ p_3^- \end{pmatrix} \tag{11}$$

The metasurface has been tested for three different sound pressure levels of the acoustic perturbation (100, 130 and 140 dB) and for the two positions of the source (upstream and downstream of the sample). As shown in Fig.4, the transmission coefficient is consistent for all the tested cases, with minor changes at high SPL. Figure 5 shows the

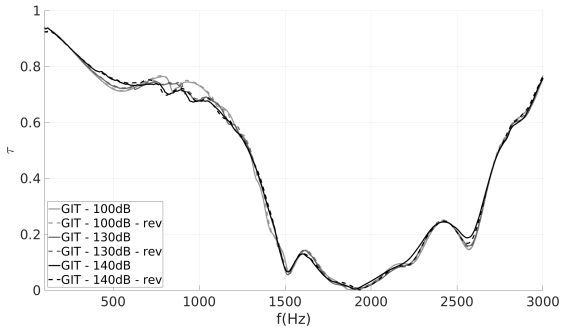

Figure 4. Transmission coefficient τ for the metasurface in the tube. Solid and dashed lines show the results for upstream and downstream source positioning, respectively, at 100, 130 and 140 dB.

comparison between the numerical prediction and the experimental results. Both the experiments and the simulations show the metasurface producing a significant loss in the transmission in the band 1000 Hz<f<2500 Hz, with a low-frequency peak around 750 Hz. The metafluid model produces results comparable to the narrow region and lossless simulations. Losses coherently have the strongest effect in the first cell, which has the longest and tightest coiled channel. Numerical results compare fairly well with experiments, although some discrepancies can be observed. The absorption peaks given by the first cell are considerably shifted in frequency: this can be related to

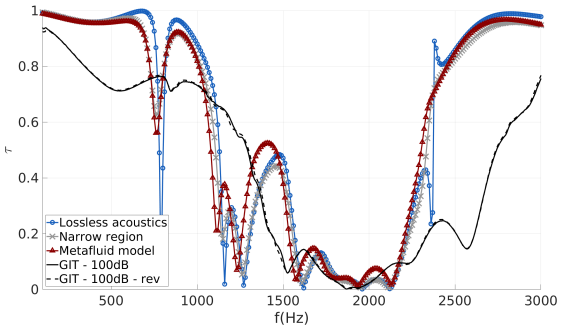

Figure 5. Transmission coefficient τ for the metasurface in the tube. Blue, red and grey lines are obtained with simulations using lossless linear acoustics, a metafluid or a narrow region lossy model, respectively, representing the metasurface's cells. Black solid and dashed lines represent the experimental results for the two positions of the acoustic source in the tube.

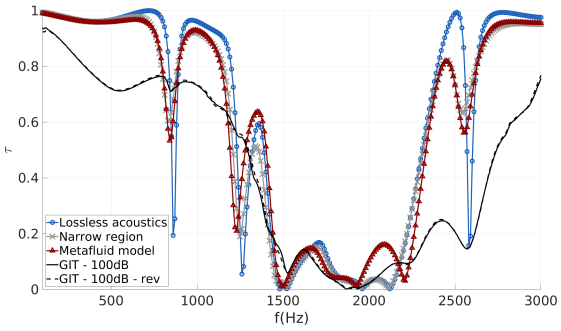

Figure 6. Transmission coefficient τ for the metasurface in the tube with modified sizes. The values of t and l are increased of Black solid and dashed lines represent the experimental results for the two positions of the acoustic source in the tube.

manufacturing uncertainties as a small difference in the height and length of the cell walls can produce a sensibly different total length for a cell with several foldings. This is proven by Fig.6, where w and t are increased by 0.5mm and 0.25mm, respectively, for the first cell, 0.25mm and 0.5mm for the second cell, and 0.5mm and 0.5mm for the third. The strongest effect can be noted on the second absorption peak of the first cell, which is pushed towards the

high frequency and appears around 2500Hz. The same shift toward higher frequency is obtained for the peak of the third cell that merges with the others around 1500Hz.

4. FINAL REMARKS

The metasurface introducing local phase-delay gradients was originally conceived for exterior acoustics metabehaviours such as steering or focusing of the reflected acoustic waves. The original design involved eight different cells, each one able to reflect the incident wave with a controlled phase delay compared to the reflection of a rigid boundary. The delay introduced by each cell is equally spaced in the complete range $0-2\pi$, such that the cells can be used as a base to build metasurfaces whose reflected field is characterized by desired (approximated) delay profiles and hence acoustic response. One of the easiest ways to introduce a delay in the reflected acoustic field is to make the incident wave interact with a resonator. At the resonant frequency, the phase delay in the reflected field is $\pi/2$, but outside of the resonance, the phase is modulated. The design strategy of the metasurface described above naturally produces a set of eight resonators with different resonance frequencies, with the aim to have cells that give different delays at the metasurface design frequency. When the eight cells are placed side by side as a wall lining in a duct, the metasurface performs a new task different from the one they were originally designed for, acting as a multifrequency liner. The transmission loss obtained numerically predict fairly well the experimental results, although with some differences. Manufacturing plays an important role in the experiments, with uncertainties and tolerances that can lead to results sensibly different from numerical simulations for small deviations from the nominal sizes.

5. ACKNOWLEDGMENTS

The authors would like to thank Dr. Thomas Humbert and Dr. Yang Meng for their advice on experimental procedures.

6. REFERENCES

[1] W. S. Weiglhofer and A. Lakhtakia, *Introduction to Complex Mediums for Optics and Electromagnetics*. SPIE Publications, 1999.

[2] T. J. Cui, D. Smith, and R. Liu, *Metamaterials*. Springer, 2010.

[3] Y. Ding, Z. Liu, C. Qiu, and J. Shi, "Metamaterial with simultaneously negative bulk modulus and mass density," *Phys. Rev. Lett.*, vol. 99, p. 093904, Aug 2007.

[4] N. Cselyuszka, M. Sečujski, and V. Crnojević-Bengin, "Novel negative mass density resonant metamaterial unit cell," *Physics Letters A*, vol. 379, no. 1, pp. 33 – 36, 2015.

[5] J. B. Pendry, "Negative refraction makes a perfect lens," *Physical review letters*, vol. 85, no. 18, p. 3966, 2000.

[6] T. Brunet, A. Merlin, B. Mascaro, K. Zimny, J. Leng, O. Poncelet, C. Aristégui, and O. Mondain-Monval, "Soft 3d acoustic metamaterial with negative index," *Nature Materials*, vol. 14, p. 384, Dec. 2014.

[7] A. Climente, D. Torrent, and S.-D. J., "Sound focusing by gradient index sonic lenses.," *Applied Physics Letters*, vol. 97, pp. 104103:1–3, 2010.

[8] Y.-F. Zhu, X.-D. Fan, B. Liang, J. Yang, J. Yang, L.-l. Yin, and J.-C. Cheng, "Multi-frequency acoustic metasurface for extraordinary reflection and sound focusing," *AIP Advances*, vol. 6, no. 12, p. 121702, 2016.

[9] A. Norris, "Acoustic cloaking theory.," *Proceedings of the Royal Society A: Mathematical, Physical and Engineering Sciences*, vol. 464, pp. 2411–2434, 2008.

[10] X. Huang, S. Zhong, and O. Stalnov, "Analysis of scattering from an acoustic cloak in a moving fluid.," *Acoust Soc Am.*, vol. 135, pp. 2571–2580, 2014.

[11] C. García-Meca, S. Carloni, C. Barceló, G. Jannes, J. Sánchez-Dehesa, and A. Martínez, "Space-time transformation acoustics.," *Wave Motion*, vol. 51, pp. 785–797, 2014.

[12] U. Iemma and G. Palma, "Aeroacoustic design of metafluid devices," in *24th International Congress on Sound and Vibration 2017, ICSV 2017: London Calling*, 2017.

[13] U. Iemma and G. Palma, "On the use of the analogue transformation acoustics in aeroacoustics," *Mathematical Problems in Engineering*, vol. vol. 2017, p. 16 pages, 2017. Article ID 8981731, doi:10.1155/2017/8981731.

[14] U. Iemma and G. Palma, "Analogue transformation acoustics in aeronautics," in *INTER-NOISE 2017 - 46th International Congress and Exposition on Noise*

Control Engineering: Taming Noise and Moving Quiet, vol. 2017-January, Institute of Noise Control Engineering, 2017.

[15] U. Iemma and G. Palma, "Convective correction of metafluid devices based on taylor transformation," *Journal of Sound and Vibration*, vol. 443, pp. 238 – 252, 2019.

[16] U. Iemma and G. Palma, "Design of metacontinua in the aeroacoustic spacetime," *Scientific Reports*, vol. 10, p. 18192, 2020.

[17] S. H. Lee and O. B. Wright, "Origin of negative density and modulus in acoustic metamaterials," *Phys. Rev. B*, vol. 93, p. 024302, Jan 2016.

[18] M. Dubois, C. Shi, Y. Wang, and X. Zhang, "A thin and conformal metasurface for illusion acoustics of rapidly changing profiles," *Applied Physics Letters*, vol. 110, no. 15, p. 151902, 2017.

[19] Y. Li, X. Jiang, R.-q. Li, B. Liang, X.-y. Zou, L.-l. Yin, and J.-c. Cheng, "Experimental realization of full control of reflected waves with subwavelength acoustic metasurfaces," *Phys. Rev. Applied*, vol. 2, p. 064002, Dec 2014.

[20] G. Palma, F. Centracchio, and L. Burghignoli, "Optimized metamaterials for enhanced noise shielding of innovative aircraft configurations," in *Proceedings of the 27th International Congress on Sound and Vibration, ICSV 2021*, jul 2021.

[21] G. Palma and L. Burghignoli, "On the integration of acoustic phase-gradient metasurfaces in aeronautics," *International Journal of Aeroacoustics*, vol. 19, no. 6-8, pp. 294–309, 2020.

[22] G. Palma, L. Burghignoli, F. Centracchio, and U. Iemma, "Innovative acoustic treatments of nacelle intakes based on optimised metamaterials," *Aerospace*, vol. 8, no. 10, 2021.

[23] M. Kadic, T. Bückmann, R. Schittny, P. Gumbsch, and M. Wegener, "Pentamode metamaterials with independently tailored bulk modulus and mass density," *Phys. Rev. Applied*, vol. 2, p. 054007, Nov 2014.

[24] A. Norris, "Acoustic metafluids.," *The Journal of the Acoustical Society of America*, vol. 125, pp. 839–849, 2009.

[25] P. Allan D., *Acoustics – An Introduction to its physical principles and applications*. Acoustical Society of America, 1994.

[26] M. E. D'Elia, T. Humbert, and Y. Aurégan, "On articulated plates with micro-slits to tackle low-frequency noise," *Acta Acustica*, vol. 5, p. 31, 2021.

[27] Y. Aurégan, M. Leroux, and V. Pagneux, *Measurement of Liner Impedance with Flow by an Inverse Method*. 2004.